JOURNAL OF MATERIALS SCIENCE **39** (2004) 7285–7294

Liquid metal model experiments on casting and solidification processes

A. CRAMER*, S. ECKERT, V. GALINDO, G. GERBETH, B. WILLERS, W. WITKE
Forschungszentrum Rossendorf, MHD Department, P.O. Box 510119, D-01314 Dresden, Germany
E-mail: a.cramer@fz-rossendorf.de

This paper is concerned with laboratory studies using liquid metals with $T_{\text{melt}} \leq 300^{\circ}\text{C}$ to model the flow of metals in industrial processes. Considering three selected examples the main features of such cold models are described. In the first instance we examine an aluminium alloy investment casting process. The requirement of reducing high flow velocities was achieved by the application of a static magnetic field. Local velocity measurements as well as integrated flow rate determination were carried out using eutectic InGaSn ($T_{\text{melt}} = 10^{\circ}\text{C}$). Secondly, model experiments were performed on the electromagnetic stirring of liquid metals in a cylindrical cavity. We applied a rotating magnetic field (RMF) and a travelling magnetic field and recorded flow maps by means of ultrasonic Doppler velocimetry. With the goal of an efficient 3D-mixing, measurements were made using a combination of both field types with promising results. Thirdly, we report on systematic studies of the effect of an RMF on the solidification of a PbSn alloy. Directional solidification experiments demonstrate the influence of the electromagnetically driven convection on the resulting microstructure.

1. Introduction

During the last decades numerical simulations have become an important tool in industry and research to study convective structures and the properties of the related heat and mass transfer. To determine the extent to which these numerical simulations are valid, experiments were done mostly on water because adequate and reliable measuring techniques exist that are commercially available. A transfer of these results to liquid metal flows is hindered by the demand to meet the relevant values of the characteristic non-dimensional parameters such as Reynolds-, Grashof-, Prandtl-, and Hartmann-numbers. In the particular cases where temperature gradients, free surfaces, two-phase flows or exposure to electromagnetic fields are involved the water experiments fail or turn out to be even meaningless. Thus, on the one hand experiments with liquid metals are indispensable. On the other hand they suffer from the lack of available measuring techniques.

Industrial scale experiments with hot metallic melts ($T \geq 700^{\circ}\text{C}$) are extremely difficult to perform and may become formidable expensive. To overcome this huge effort we propose small scale model experiments using low melting point metallic melts for detailed investigations of flow problems. This approach is supported by the availability of appropriate measuring techniques. In the temperature range up to 300°C various methods allow the determination of almost any flow quantities such as mean velocities, turbulent fluctuations or two-phase flow parameters [1]. Besides the established potential difference probes the upcoming ultrasonic Doppler velocimetry (UDV), which is briefly discussed in the following Section, permits the determination of local velocities.

A multitude of metals and metallic alloys with a melting point below 300°C exist allowing an optimal choice of the model fluid for any real industrial flow problem. Not until the numerical simulations are validated by such small-scale, well-measured liquid metal models should they be used to calculate the real-scale industrial case.

This paper presents three examples of this strategy. In the next but one Section the control of an aluminium investment casting process by means of a magnetic field is demonstrated. The requirement was to reduce the high flow velocities during the early stage of the filling process. As static magnetic fields are known to damp the flow of electrically conducting media, an optimised solution of the strength and the geometry of the field, and its position at the caster was sought. This task was fulfilled by a combination of numerical simulation of the flow field and an isothermal physical modelling of the casting process. UDV was applied for the local velocity measurements, and the flow rate was determined independently by employing the contact-less transmitter technique [1]. The use of eutectic InGaSn which is

*Author to whom all correspondence should be addressed.

liquid at room temperature permitted to set up an easy to build and flexible perspex model.

In Section 4 we are concerned with the electromagnetic stirring of metallic melts. The convective structures created by all types of alternating magnetic fields are believed to be well understood. In practice, due to economic reasons, the fields are never homogeneous and isotropic as commonly assumed in the frame of theoretical investigations. Superimposition of different field types to break the symmetry of rigid two-dimensional flow structures may be interpreted as a greatly increased non-homogeneity which cannot be treated by analytical theory. Such combined magnetic fields are expected to have a high efficiency regarding the melt mixing. We provide results obtained in cylindrical vessels exposed to rotating and/or travelling magnetic fields. The capabilities of UDV permitted mapping the flow in an entire section throughout the whole container.

Finally, studies concerning the influence of a magnetically driven convection on the solidification of a PbSn alloy are reported in Section 5. In particular, that process serves as an instance of the necessity for reliable physical modelling. The numerical calculation of the flow is exceedingly difficult primarily, but not only, because of the two-phase problem (mushy zone) and the moving boundary (solidification front). Nucleation and growth processes are influenced by the local heat transfer. A fully coupled numerical treatment, including a code to simulate the solidification, is unpromising unless interim results can be compared with experimental data. What information can be acquired from the bulk of a hot and aggressive melt in the real process? In practise, only data from the ready-made product like metallography, hardness or micrographs are available when the ingot has cooled down. Delivery of interim results means that the data determining the mechanisms are needed to be known. Liquid metal model experiments in combination with the respective measuring techniques have the potentiality to provide at least some of them.

2. Ultrasonic doppler velocimetry

Due to the principle of its operation this technique delivers an entire velocity profile along the ultrasonic beam and is thus suitable for enhanced measuring tasks such as flow mapping. Since we used UDV intensively in this study, questions about its accuracy and reliability have to be addressed. With its roots in the medical applications ultrasound was adopted some 20 years back as a general purpose device to measure velocities in the field of fluid engineering with the particular benefit to work also in opaque media. Commencing with the pioneering work of Takeda [2] up to the present time only a few publications exist describing the use of UDV to measure velocities in liquid metals. From our own experience it turns out that the spatial resolution does not compare with that of Laser Doppler Anemometry which is the state of the art method for transparent media. Nevertheless, depending on the specific measuring task, there may be a tradeoff between accuracy and sample rate via the integration time allowed for reproducibility in the typical range down to 1 mm/s on the one hand and profile repetition rates up to 40 Hz on the other hand. It is still unclear if this technique is appropriate for the measurement of turbulent flow properties, but at least changes of the mean flow are detectable. For further details, in particular the applicability to liquid metal flows, we refer to Cramer [3] and the references therein. Note that the application of suitable ultrasonic wave-guides allows to measure velocities under higher temperature conditions. Successful applications to melts like CuSn or Al in the range of $T \approx 750^{\circ}$C have recently been reported [4].

3. MHD control of an aluminium investment casting process

The investment casting process using the lost-wax method allows for a high variability of shapes and guarantees high accuracy and excellent surface quality. The objective of our investigation was to control the velocity of the aluminium melt during the pouring process. The main problem is the occurrence of large velocity values in the beginning of the casting process, leading to an accumulated generation of vortices inside the pouring channel. A high rate of turbulence in the flow is supposed to entail the transport of impurities, oxides, or gas bubbles from the walls and the free surface into the bulk of the casting. As a result the mechanical properties of the casting products are deteriorated. In order to reduce the melt velocity we applied a static transverse magnetic field. In particular, the task was to propose a design for a magnetic system and to find its optimum position at the casting unit.

Numerical calculations were performed using the commercial finite element code FIDAP (FLUENT Inc.). The term for the electromagnetic Lorentz force was implemented by a user-defined subroutine. Additionally, an equation for the electric potential was solved. Fig. 1 shows an example for calculations made for a simple geometry consisting of a vertical pouring funnel, a horizontal rectangular channel and a cylinder modelling the casting mould. Here, the flow of liquid aluminium without magnetic field was compared to the situation where a transverse static field of 0.5 T was positioned at the end of the pouring funnel covering the 90° bend, too. The braking effect of the magnetic field on the flow velocity in the mid-plane of the considered channel was obvious.

In parallel with the numerical calculations, model experiments with the eutectic alloy InGaSn were conducted. Different types of perspex pattern were produced, which gave us a flexibility in finding an optimal geometry and magnetic field position. One example is depicted in Fig. 2. The height of the vertical pouring funnel was 400 mm, and the flow channel had a rectangular cross section of 30 mm by 5 mm. An electromagnetic system created a steady magnetic field up to a maximum induction of 0.9 T. The bottom part of the pouring funnel was chosen as the position for the magnetic field because the numerical simulations as well as initial experiments have shown that the maximum values of the velocity were to be expected in this region.

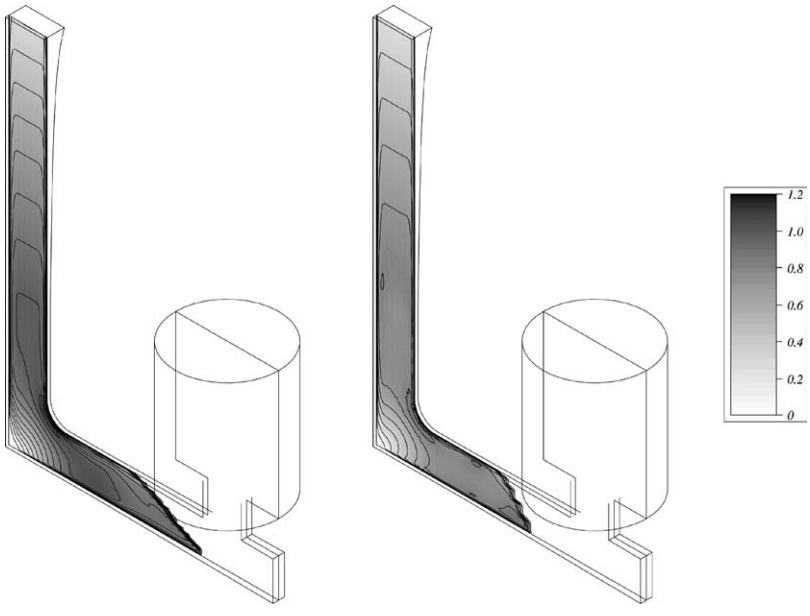

Figure 1 Numerical results of the velocity of a pouring flow of liquid aluminium. Left: without magnetic field; right: transverse field. Velocities are given in m/s.

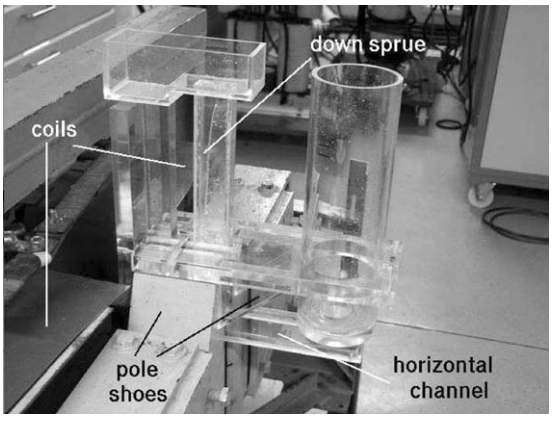

Figure 2 Perspex model of a casting pattern positioned at the magnetic field system.

In the course of the pouring experiments velocity profiles were acquired by means of UDV. While keeping the ultrasonic transducer attached to the channel wall these profiles were determined along the vertical pouring funnel as well as along the horizontal channel. The integral flow rate was also measured using an inductive flow meter [1]. The transparency of the wall material allowed for visual observations of the filling process of the perspex pattern. By this visual assessment and from the UDV data the undesirable occurrence of gas bubbles inside the flow channel could be detected.

The experimental investigations demonstrate impressively the effect of the static field on the velocity of the pouring liquid metal. Fig. 3 shows UDV measurements obtained in the vertical pouring funnel and in the horizontal channel respectively. The application of the magnetic field always reduces the mean velocities. The most significant decrease was observed for the peak value at the beginning of the pouring process as can be seen in the left graph of Fig. 3. To the right the typical signal of a bubble passing the measuring volume can be seen.

Coinciding with our impression from visual observations, the UDV measurements in the funnel reveal that the damping is not restricted to the mean flow. When exposed to the magnetic field the velocity fluctuations became smaller, too, at least in the vicinity of the magnet. It is obvious from the left graph in Fig. 3 that the amplitude of the remaining fluctuations in the UDV signals compare between the two different values of the magnetic induction, indicating that the much weaker

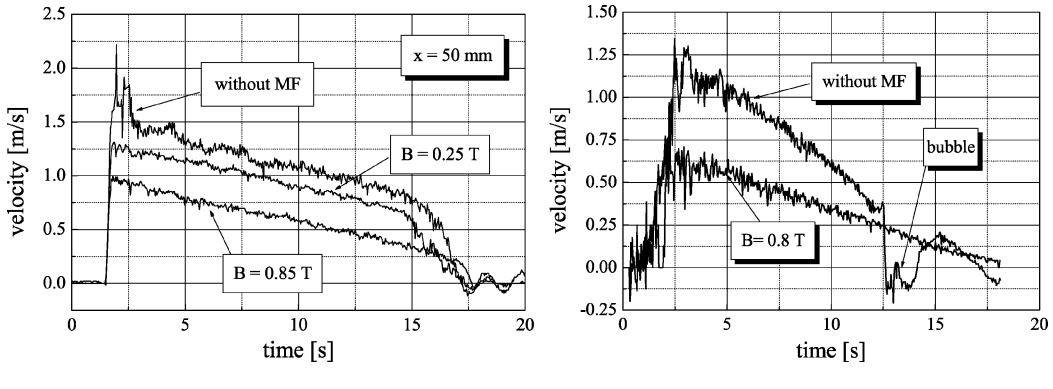

Figure 3 UDV velocity measurements for various values of the magnetic induction. Left: in the vertical funnel at 50 mm distance from the bottom; right: in the horizontal channel below the joint to the cylinder simulating the mould, a bubble is crossing the ultrasonic beam.

strength of 0.25 T already damps most of the velocity fluctuations. The remaining level of fluctuations in both these signals is apparently determined by the noise of the UDV technique. At the location far downstream in the horizontal channel (right part of Fig. 3) no significant difference in the fluctuation level was detected. However, the number of gas inclusions that are trapped in the down sprue and the adjacent region in the horizontal channel can be significantly reduced by application of a static magnetic field.

In order to quantify the performance characteristics of the magnetic field the dependence of the flow rate on the induction was studied both experimentally and numerically. Fig. 4 shows how the ratio of the flow rate in the presence of a static magnetic field to the flow rate without a field varies with the strength of the applied magnetic field. The experimental data obtained from the model experiments showed a fair agreement with the results predicted by the numerical calculations, thereby validating the numerical code.

The validated numerical code was an important tool in the design of the prototype of a magnetic system for the real aluminium investment casting process. To a first approximation such an up-scaling is effected by keeping constant the interaction parameter, N, which is the governing dimensionless number.

$$N = \frac{Ha^2}{Re} = \frac{\sigma B^2 L}{\rho u} \qquad (1)$$

The Hartmann number Ha measures the strength of the applied magnetic induction B and Re is the Reynolds number. As determining quantities, the electrical conductivity σ and the density ρ of the fluid, the channel width L in the direction of the magnetic field, and the typical velocity u remain, besides B, in the rightmost expression of Equation 1. A magnetic system based on this similarity criterion and further numerically optimised with regard to geometric details was manufactured and successfully installed at an industrial facility. Exposing the magnet for a few seconds in the beginning of the process, only, allowed to reduce the velocity peaks drastically without prolonging the overall casting duration significantly. The statistics of a multitude of cast units showed a clear tendency towards reduced oxide entrapment due to the magnetic field influence.

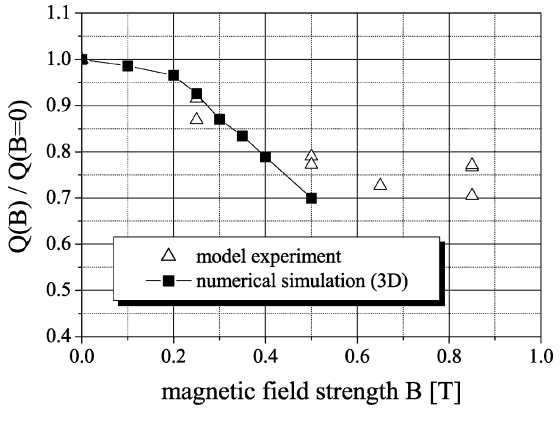

Figure 4 Comparison of numerical and experimental results regarding the flow rate as a function of the magnetic field strength (related to the flow rate obtained with $B = 0$).

4. Investigation of the flow structures in rotating and travelling magnetic fields

4.1. Motivation

Commercially available stirrers are equipped either with a rotating magnetic field (RMF) or a linear arrangement of coils supplying a travelling magnetic field (TMF). Often the homogenisation created by these devices falls behind expectations. In the last decades much effort has been spent to answer the question why the efficiency is so small.

A quantitative description of the mixing effect has to be based on the distribution of the respective concentration of species. To be more precise, one would be concerned with the temporal evolution thereof which is the transport of a passive scalar. In [5] a two-dimensional problem was studied assuming that the velocity fluctuations are homogeneous and isotropic. The continuation in a more recent work [6] aims at a deeper insight into how the observed stretching and folding of fluid elements affect the mixing. Measurements of mixing rates, defined as the rate of decay of the root mean square concentration inhomogeneity, as they relate to the flow velocity have been reported. In particular these authors studied the sequence of transitions commencing with that from laminar to time-periodic flow via period multiplying to the onset of non-periodicity. Probably their most important finding is that the breaking of spatial symmetries turned out to be the dominant feature affecting mixing.

It is noteworthy that in [5, 6] well-characterised two-dimensional flows of transparent media have been used. Employing light absorption measurements at such flat layers it is possible to determine simultaneously the dye concentration fields, velocity fields, and stretching fields. This technique is not applicable to liquid metal flows in metallurgy. From the physical point of view the turbulence characteristics are expected to be quite different owing to the third dimension present in the applied case. In practice one is once more often confronted with the everlasting problem regarding the measuring techniques for liquid metal flows. In Section 2 the new possibilities of UDV to determine the flow field have been pointed out, but any attempt to measure concentrations in liquid metals is a hopeless venture.

To be self-consistent a brief explanation of the mean flow is given in the next Subsection, which includes measurements of the flow field displayed in the format of a flow map in a meridional section through the centre of the container. It is followed in the next but one Subsection by an equivalent representation of the velocity fluctuations. As we shall see, the breaking of symmetry which is being made responsible for an enhanced mixing in [6] can already be detected in the case of stirring by one field type alone. Finally, by utilizing the non-axisymmetric Lorentz force distribution provided by the combination of an RMF and a TMF stronger symmetry breaking of the flow is sought.

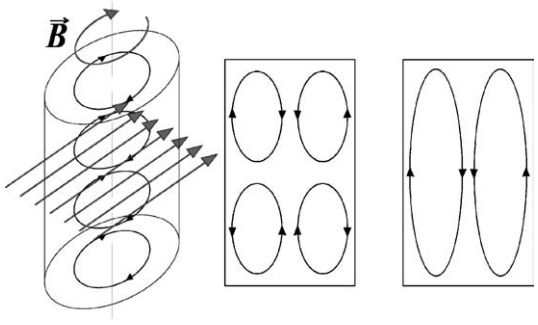

Figure 5 Sketch of the mean flow structures in an RMF (leftmost 2 figures) and a TMF. The swirl created by the RMF (left) has almost no axial variation except in the close vicinity to the top and the bottom. In most applications the induction is kept constant with respect to the vertical axis, too. Having the same sense of rotation the angular velocity of the field is quite different from that of the flow. Even for small scale laboratory experiments it becomes large in comparison. The 2 rightmost figures depict the toroidal flow structures in a meridional section. The sense of rotation in the RMFs secondary flow (middle) does not depend on that of the magnetic field. The rightmost figure depicts the case of an upward travelling magnetic field.

4.2. Mean flow

Both the RMF and the TMF applied to a metallic melt inside a closed container drive mainly rigid 2D flow structures [7, 8]. In the case of the RMF the liquid metal rotates azimuthally about the vertical axis along with the vector of the magnetic field. In the linear inductor the fluid follows the travelling field at the rim of the container, and closes to a toroidal structure in the centre where the magnetic field is much weaker. A noticeable mixing via material transport perpendicular to the mean velocity vector is to be expected only in the highly turbulent regime. For a discussion of the mixing effect in terms of flow structures it is important to note that the fluid motion generated by an RMF differs in principle from the TMF driven one as all velocity components are non-zero already in the laminar case. A weak secondary flow occurs due to the no-slip condition at the vertical end-walls, and is believed to be a factor of 5 to 7 times smaller than the azimuthal velocity scale. This meridional structure consists of two tori with a common flow directed outwards from the centre to the rim between them, and an inward flow at the top and the bottom of the container closing conformably along the side-walls and the axis. For a comprehensive overview of the RMF-driven flow we refer to Davidson [8].

In the experiments a magnetic system was used that allowed for an independent variation of the field strengths and frequencies of an RMF and a TMF respectively. Recording of the fluid velocities was done by UDV. The ultrasonic sensor was mounted on a traversing unit at the top of the container with its axis perpendicular to the lid, thereby providing the vertical velocity component. As easy to handle liquid metals, InGaSn and mercury were used. The cavity aspect ratio was fixed to 1.5. The size of the melt volume, which was 60 mm in height and 20 mm in radius, was chosen according to that region where the magnetic fields are nearly homogeneous.

The first set of experiments was devoted to the secondary flow driven by an RMF. Recording of the vertical velocity component along the vertical z-axis was done while moving the sensor in a radial direction. Fig. 6 depicts the iso-lines of constant velocity of two such sections in the r, z-plane. An arbitrary r-direction was chosen for the first section whereas for the second contour plot it was rotated by 90° while all other parameters were kept constant. Even for the low induction of 9.2 mT the boundary layer type of the flow was well established. In agreement with theory the main flow eddies could be identified from the strong up- respectively down-streams at the rim. The radial velocity gradients were less pronounced in the lower part of the container which is easily explained by the divergence of the ultrasonic beam leading to a loss of spatial resolution. Whereas the flow field in the upper half seemed fairly axi-symmetric this no longer held for the lower part. The strong down-streams obtained there contradict everything known about the recirculation of RMF-driven flows. Even though they should not be present at all, the highest absolute values of the velocity were found there. The different radial positions of these down-streams in

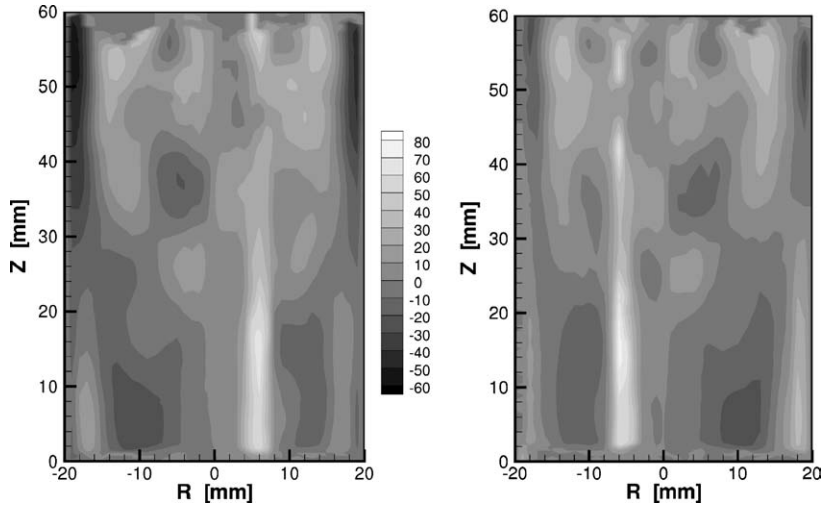

Figure 6 Iso-contour plots of the vertical velocity component of a flow driven by a RMF ($f = 50$ Hz, $B = 9.2$ mT, $Ta = 9.5 \times 10^6$). The legend of the velocity scale is in mm/s, positive values represent a downward flow. Left: radial movement of the transducer along an arbitrary axis; right: radial direction changed by 90°.

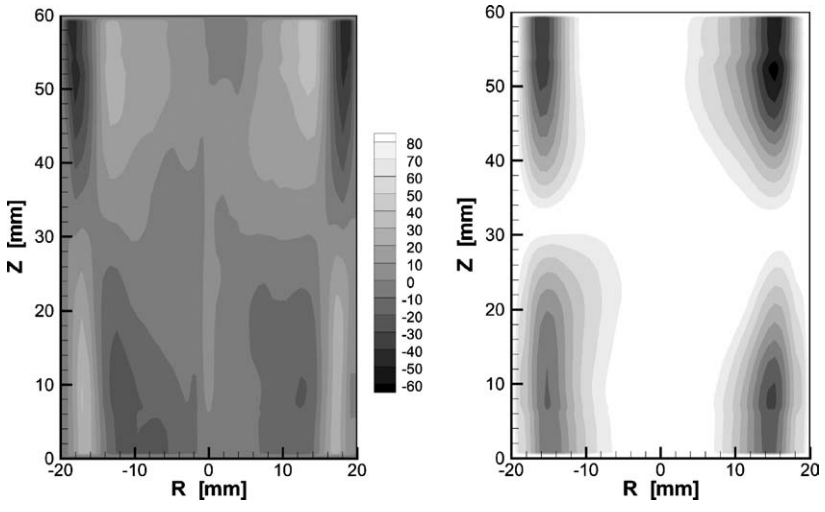

Figure 7 The same experiment as in Fig. 6 with precisely adjusted container and magnet. Left: iso-contours of the vertical velocity component; right: absolute value of the stream function numerically integrated from the measured vertical velocity distribution.

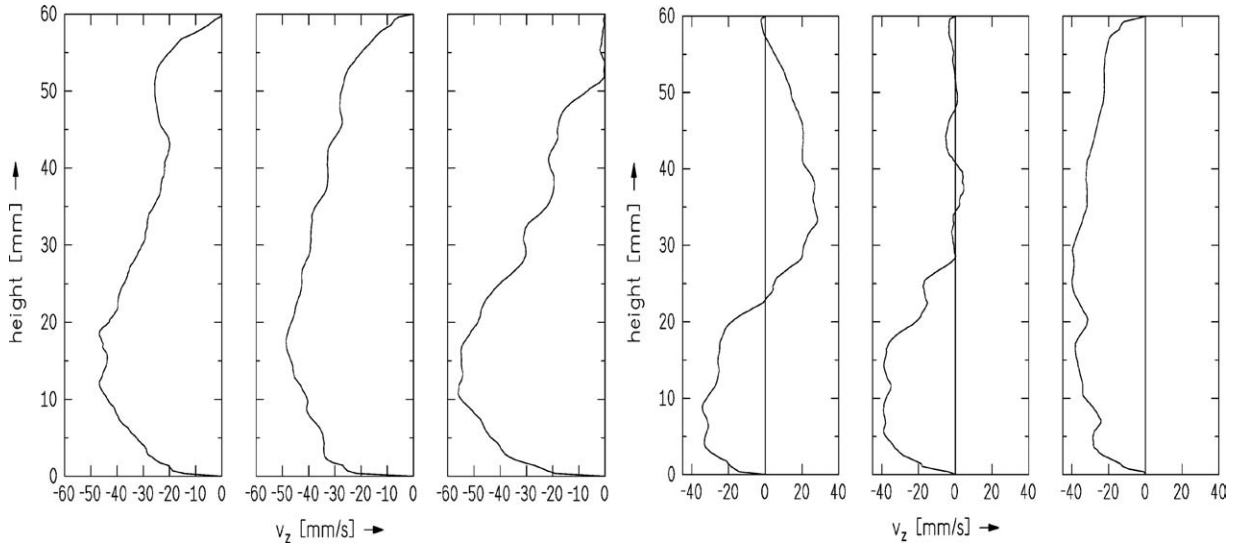

Figure 8 Snapshots of vertical velocity profiles. Left: upward directed TMF ($B = 7$ mT, $f = 70$ Hz, $Ta = 9.7 \times 10^6$) measured at a radial coordinate of 18 mm; right: combination of a downward travelling field with same parameters as in left graph and an RMF ($B = 3.5$ mT, $f = 70$ Hz, $Ta = 2.4 \times 10^6$), measured in the centre.

the two contour plots additionally indicate the strong asymmetry of the flow. A closer look at Fig. 6 shows the deviation from axi-symmetry in the upper half of the vessel, too, as the absolute values of the up-stream at the rim are smaller in the right plot.

The experiment was repeated with a different combination of the magnetic field induction and frequency (7.5 mT, 70 Hz, $Ta = 8.8 \times 10^6$). The measured velocities should decrease only slightly as the velocity scales as $O(Ta^{2/3})$ with the governing dimensionless parameter Ta which is the magnetic Taylor number given by

$$Ta = \frac{\sigma \omega B^2 L^4}{2\rho\nu^2} \qquad (2)$$

where ν is the kinematic viscosity and $\omega = 2\pi f$. This tendency was confirmed by the experiment, but the asymmetry remained.

One possible explanation for this observed asymmetry is that the meridional flow may be highly sensitive to tilting. The misalignment of the magnet turned out to be negligible and the tilting of the container was hardly half a degree. For another repetition of the experiment both the container and the magnet were carefully adjusted by means of a precision spirit level. The convective pattern shown in Fig. 7 is almost axi-symmetric. For that more stable and reproducibly measurable flow it was possible to integrate a stream function numerically from the measured axial velocity distribution, the absolute value of which is presented in the right part of Fig. 7. At this stage it may be concluded that such precise conditions are hardly realisable under rough industrial conditions and thus the flow structure in a real liquid metal process may be very different from what it is believed to be.

For the TMF-driven flow it seemed to be impossible first to record the expected single torus 2D flow structure. The acquired UDV profiles changed drastically in time. Even averaging many velocity profiles sampled consecutively produced quite different results. Only upon sampling each radial coordinate over a very long time, which was several tens of seconds in that

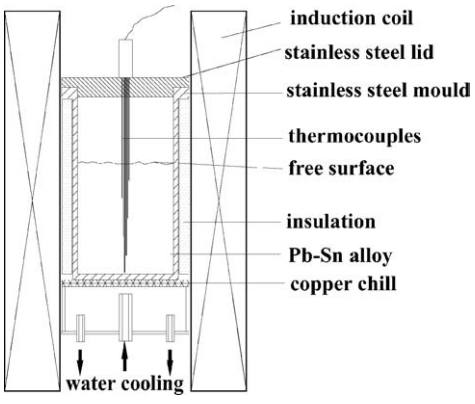

Figure 9 Schematic view of the setup used for the solidification experiments.

case, an averaged velocity distribution resembling the expected single torus was obtained.

4.3. Velocity fluctuations

From large eddy simulations and potential difference measurements at one fixed coordinate [9] it has recently been observed for the single-phase pulsating magnetic field (PMF) that the flow undergoes nearly harmonic velocity oscillations with a frequency of the order of 0.1 Hz. Several preliminary experiments with a PMF were performed and such low frequency velocity fluctuations were confirmed. The UDV measurements on a TMF-driven flow suggested that similar oscillations may be present. Using an upward travelling field, long-term series were recorded in a region adjacent to the rim. Three representative snapshots from the time-series are displayed in the left part of Fig. 8. The large-scale fluctuations depicted here are located in the upper half of the vessel, but they can be found at every vertical coordinate.

Processing of the time-series data showed that these fluctuations take place on a time scale of the order of 10 s. When applying the RMF no similar changes within the velocity profiles have been found, no matter what combination of frequency and field strength was used. Seemingly the TMF and the PMF are similar regarding the occurrence of low frequency oscillations which cannot be termed turbulence in the classical sense, but can be expected to have a large influence on transport and mixing properties of the flow. A pictorial description of the flow might be a more or less ever-changing structure that averages, on a very long timescale only, to the topology predicted by theory to be the mean convective structure driven by a TMF. It is even likely that this mean velocity distribution is never exactly realised by the flow at any instant in time.

However, we found no change of the velocity, from large positive to large negative velocity values, anywhere in the fluid volume. Such a temporal behaviour of the flow, if it could be realised, can be expected to have good mixing properties. Concerning the motivation to superimpose an RMF with a TMF for the purpose of an efficient stirring, it was seemingly reasonable at first sight to use comparable field strengths so as to have an according ratio between azimuthal and meridional motion. Since the flow driven by a TMF alone was already unexpectedly non-stationary showing the desired large-scale symmetry-breaking fluctuations this initial proposal was reconsidered. Instead the interesting question about the influence of a small RMF on a mainly TMF-driven convection arose. For the snapshots in the right part of Fig. 8 the direction of the TMF was chosen downwards in order to have the counteracting part of the secondary flow driven by the RMF in the upper part of the container where the spatial resolution of the sensor was better. The measurements with combined fields showed that in the upper part of the container the flow changed continually from positive to negative velocities of comparable absolute value. This region of sign-reversal, which strongly breaks the symmetry of the flow, extended beyond the equator of the container. Thus, a strong mixing in the whole container could be assumed.

It is worth noting that the significantly weaker RMF had such a big influence on the flow structure. The RMF mainly drove an azimuthal motion and only its much weaker secondary flow interacted directly with the one driven by the TMF. The time-dependence of the motion created by the combined field was harmonic to a high degree with a time scale of the lowest-frequency mode typically as low as that found in the PMF and the TMF alone.

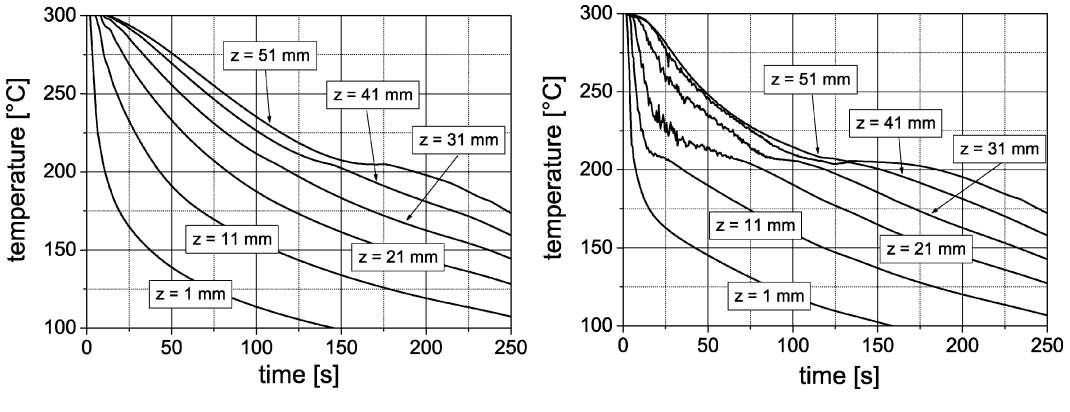

Figure 10 Cooling curves obtained inside a Pb85 wt%Sn alloy solidified directionally. Left: without electromagnetic stirring; right: under the influence of an RMF ($B = 10$ mT, $f = 50$ Hz, $Ta = 1.7 \times 10^7$).

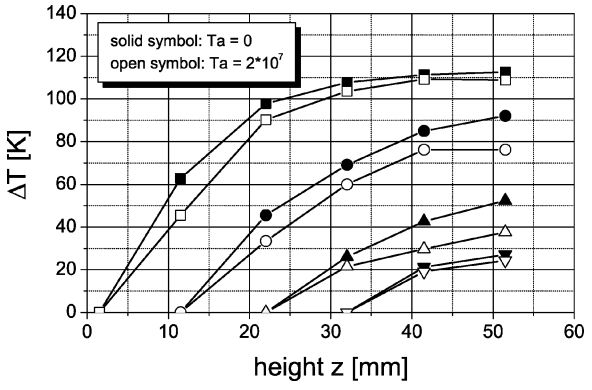

Figure 11 Influence of electromagnetic stirring on the temperature profiles. Temperature differences plotted on the abscissa are measured between a certain sensor and the consecutive one within the axially aligned positioning. As the value for the axial position of that couple the coordinate of the lower sensor is used on the ordinate. The 4 pairs of curves represent snapshots at the instant in time when the solidus temperature was detected at the thermocouple closest to the bottom of the container.

5. Solidification of PbSn under the influence of a rotating magnetic field

It is known that the microstructure of metallic alloys can be significantly affected by convection [10, 11]. If a magnetic field varying in time is applied to the liquid phase during solidification it establishes a flow field which in turn influences the nucleation and growth processes. The experiments presented here sought a strategy to refine the microstructure of castings by an optimal combination of magnetic field intensity, its frequency, and the cooling rate. In addition, the physical mechanisms underlying the influence of the RMF on the solidification have been investigated.

5.1. The experimental setup

A Pb85 wt%Sn alloy was directionally solidified using the experimental setup depicted in Fig. 9. The melt was contained in a cylindrical stainless steel crucible having an inner diameter of 50 mm and a height of 60 mm. Between the melt surface and the steel lid a 30 mm wide gap remained which was occupied by the ambient air. Thus the heat extraction from the solidifying alloy by a water-supplied copper chill, mounted beneath the container bottom, was in the vertical direction. Adjusting a high water flow rate kept the copper plate at a constant temperature of 20°C. An electrical heater established a superheat of 90 K above the liquidus temperature of the PbSn alloy prior to positioning the crucible on the chill. Thermal insulation of the side-walls of the crucible minimised radial heat losses. From the uniform radial temperature distribution measured in the course of the experiments it could be confirmed that no radial heat flux has to be taken into account. Heat losses across the melt-air surface were also found to be negligible. The RMF was generated by an inductor composed of 6 coils which afford field strengths up to 25 mT and a continuous frequency variation between 10 and 400 Hz. Temperature measurements during the solidification process were made by 6 chromel-alumel thermocouples at different axial positions inside the ingot. As can be seen in Fig. 9 the thermocouples were arranged along the centre axis to minimise perturbations of the flow structure. Commencing with the first one just at the bottom of the crucible the vertical distance between two adjacent thermocouples was 10 mm. Profiles of the melt velocity and the position of the solidification front were determined by the UDV method.

5.2. Results

Cooling curves obtained at different vertical positions inside the sample are shown in Fig. 10 for the case without electromagnetically driven convection, and in that when the solidifying ingot was exposed to a RMF with a field strength of 10 mT and a frequency of 50 Hz. With the RMF applied the fluctuations of the temperature signal above the liquidus temperature indicate turbulent convection in the liquid phase. As can be seen from the steeper gradient of the temperature curves in the beginning of the process the flow enhances the heat transfer.

The influence of electromagnetic stirring on the thermal profiles above the solidification is shown in Fig. 11. It is obvious that the convection equalises the temperature distribution in the liquid phase, and decreases the temperature gradient in front of the solid-liquid interface. An important parameter to characterise solidification processes is the growth velocity V of the solidification front. The duration for the liquidus

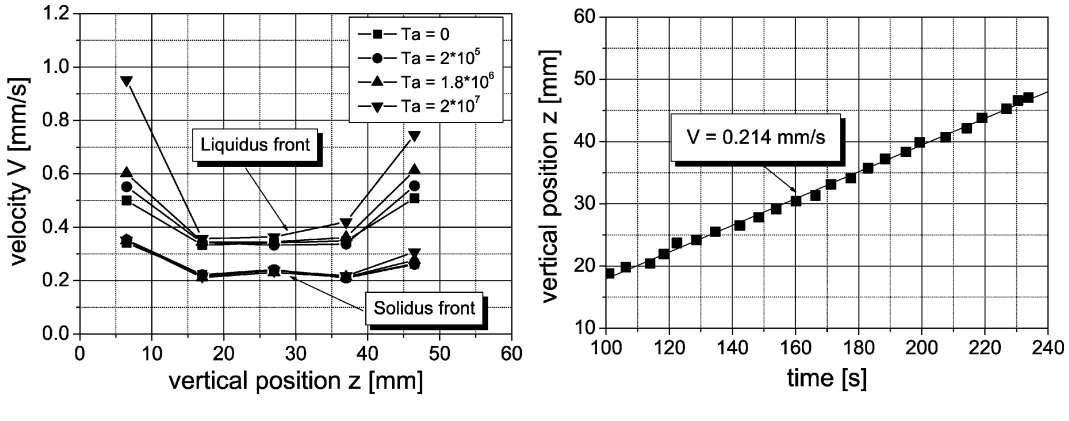

Figure 12 Growth velocities of liquidus and solidus front calculated from temperature data (left), and of the solidification front determined by UDV (right) under the influence of an RMF (right: $B = 10$ mT, $f = 50$ Hz, $Ta = 1.7 \times 10^7$).

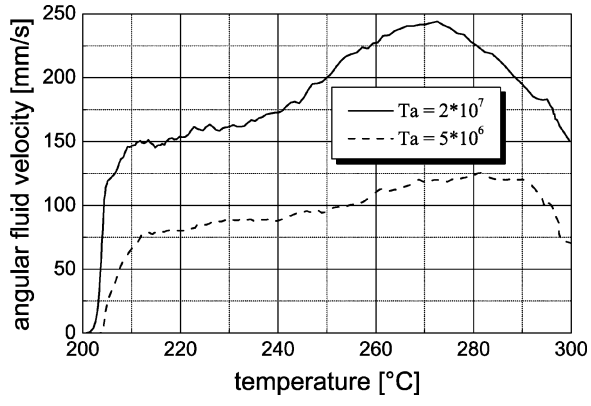

Figure 13 UDV measurements of the azimuthal velocity at $r = 20$ mm, $z = 50$ mm for two different parameters of the RMF.

respectively the solidus temperature being detected at the various thermocouple positions was used to estimate the position of the appendant front. Fig. 12 charts on the left side a higher velocity of the liquidus front, indicating an increase of the mushy zone region during the solidification process. In the bottom part of the sample an increase of the growth velocity with increasing magnetic field is observed corresponding to the enhanced heat transfer. It is also possible to determine the speed of the solidification front by UDV. For that purpose the ultrasonic sensor was installed at the free melt surface in a vertical-downward position, thus measuring the vertical velocity component. In a straightforward manner the position of the solidification front can be defined as that measuring depth where the velocity tends to zero. The speed of the moving front acquired by this method is then given by the time derivative of its vertical position which is the slope of the curve in the right side of Fig. 12. As the flow velocity measured by UDV is exactly zero not until the melt is entirely solidified at the measuring position, the speed of the front determined thereby should coincide with the solidus front. From the comparison between these two front velocities in Fig. 12 a good agreement can be stated.

Fig. 13 shows two UDV measurements of the azimuthal velocity during the solidification process as a function of the temperature. The measuring position was at $z = 50$ mm and $r = 20$ mm. In the early stage of the experiment the flow develops due to the driving action of the RMF. Jointly with the approaching solidification front the velocity decreases, and tends steeply to zero as the liquidus front ($T_L = 209°C$) passes the measurement position.

Due to the composition of the Pb85 wt%Sn alloy its microstructure is composed of primary tin-crystallites and eutectic. Specimens solidified without electromagnetic stirring showed columnar dendrites aligned with the heat flux direction. If the alloy solidifies under the influence of an RMF the microstructure changes with respect to topology and distribution (see Fig. 14). The shape of the dendrites is altered from columnar to equiaxed in direction from the bottom to the top of the specimen.

6. Conclusions

From the physical point of view a water modelling of liquid metal processing is often far removed from reality, particularly if temperature gradients, free melt surfaces or two-phase phenomena are involved. A better understanding of the flow properties and the related heat and mass transfer requires a detailed knowledge of the flow field, on account of which velocity measurements are needed. Hitherto, only very few laboratory examples for such velocity measurements exist, nothing is available for industrially relevant metallic melts.

The idea to fill in this gap is the setup of meaningful liquid metal model experiments with temperatures up to 300°C. A positive prospect of success is supported by a number of recently developed measuring techniques for that temperature range. Thereby it is possible today to model metallurgical processes in a range of the characteristic transport parameters very close to reality. Validation of numerical codes by such liquid metal models provides obviously a profound basis for an extrapolation towards the real-scale problem.

Magnetic fields are a convenient option to control liquid metal flows in a contact-less and precisely adjustable way. They provide a wide spectrum of exerting influence, spanning from flow damping to flow driving mechanisms. In many cases tailored magnetic fields can

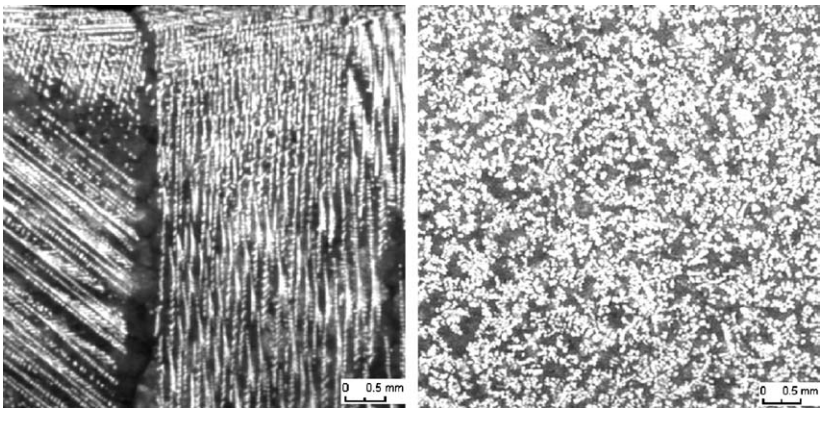

Figure 14 Microstructure of a Pb85 wt%Sn alloy solidified without (left) and with (right: $B = 7$ mT, $f = 120$ Hz, $Ta = 2 \times 10^7$) electromagnetic stirring by an RMF.

be designed specifically for the desired impact on the transport properties of the flow.

Three common industrial processes have been instanced to demonstrate the successful interaction between well coordinated physical modelling, electromagnetic flow control, and measuring techniques. The first one dealt with the design of a flow brake for the aluminium investment casting using an adapted steady magnetic field. A significant reduction of the peak velocity in the beginning of the filling process has been shown by model experiments and numerics, and has also been demonstrated in the real aluminium casting process. The second example revealed the capabilities of magnetic field design towards an efficient mixing of a metallic melt. Our approach is based on the idea to couple different flow patterns that are produced by different types of multi-phase alternating magnetic fields. The model experiments seemed to confirm the effectiveness of such a tailor-made flow control. Beyond it they delivered a more detailed insight into the sensitivity of those flows to influencing factors generally present in an industrial process. Finally, we reported on basic studies of solidification control using PbSn as model material. Application of a rotating magnetic field strongly changes the flow field close to the solidification front and thus has a wide influence on the resulting microstructure. Again, the potential of velocity measurements in combination with the recording of temperatures leads to a better understanding of these complex phenomena.

Acknowledgement

Financial support from "Deutsche Forschungsgemeinschaft" in the framework of the Collaborative Research Centre SFB 609 is gratefully acknowledged.

References

1. S. ECKERT, G. GERBETH, F. STEFANI and W. WITKE, "Measuring Techniques for Liquid Metal Velocity Measurements," in Proc. LMPC, edited by P. D. Lee, A. Mitchell, J.-P. Bellot and A. Jardin (Nancy, France, 2003) p. 261.
2. Y. TAKEDA, *Nucl. Techn.* **79** (1987) 120.
3. A. CRAMER, C. ZHANG and S. ECKERT, *J. Flow Meas. Instr.* **15** (2004) 145.
4. S. ECKERT, G. GERBETH and V. I. MELNIKOV, *Exp. Fluids* **35** (2003) 381.
5. B. S. WILLIAMS, D. MARTEAU and G. P. GOLLUB *Phys. Fluids* **9** (1997) 2061.
6. G. A. VOTH, T. C. SAINT, G. DOBLER and G. P. GOLLUB, *Phys. Fluids* **15** (2003) 2560.
7. YU. YA. MIKEL'SON, A. T. YAKOVICH and S. I. PAVLOV, *Magnetohydrodynamics* **14** (1978) 42.
8. P. DAVIDSON, *Annu. Rev. Fluid Mech.* **31** (1999) 273.
9. E. BAAKE, B. NACKE, A. UMBRASHKO and A. JAKOVICS, *Magnetohydrodynamics* **39** (2003) 291.
10. W. C. JOHNSTON, G. R KOFLER, S. O'HARA, H. V. ASHCOM and W. A. TILLER, *Trans. Mat. Soc. AIME* **233** (1996) 1856.
11. W. D. GRIFFITHS and D. G. MCCARTNEY, *Mat. Sci. Techn.* **A216** (1996) 47.

Received 10 March
and accepted 17 June 2004